An Analytical Method of Evaluating Nonuniformities in Shock Tube Flows. Part 2: Application.

Matthew Satchell *, Alex Glenn †, Peter Collen ‡, Rowland Penty-Geraets §, Matthew McGilvray ¶, and Luca Di Mare ‖
Osney Thermofluids Institute, University of Oxford, United Kingdom

Shock tube experiments are a primary means of obtaining ground test data for the hypersonic regime. Accurate characterisation of the test gas is crucial to understanding experimental results. However, characterisation of the flows produced behind the shockwave has historically proven challenging. This paper applies a methodology to calculate the shocked test gas properties using the experimentally recovered shock speed profile. Static pressure, Pitot pressure and heat transfer predictions are found to closely match the experimental data for a range of shock trajectories with both Argon and Air test gases. Thermochemical variations in the test gases are found to depend strongly upon variations in shock speed along the tube, and it is shown that characterisation of the test gases requires accommodating the influence of wave effects associated with the varying shock speed. Tube diameter is found to influence test time significantly, and also the magnitude of nonuniformities in the test gas. Location and number of shock timing stations in experimental facilities are found to play a vital role in the ability to accurately characterise the test gas of a given experiment.

I. Introduction

High speed vehicles generate non-equilibrium thermochemical effects which is directly coupled to the aerodynamics and heat transfer. Shock tubes have been a key ground test facility to explore thermochemistry by replicating the stagnation line flowfield. Although typically thought of as simple, producing clean test flow behind a constant shock speed, most real experiments in these facilities are impacted by boundary layer growth and non-ideal driver and diaphragm rupturing effects. Thus, the shock speed varies as it propagates down the tube leading to nonuniformities in the test gases of shock tubes [1–6]. The use of only the final shock speed rather than the complete shock history down the tube leads to large discrepancies in the shocked test gas flow properties [7]. As each experiment in a given facility will produce a different shock speed profile, a method of analysing the test gas properties for each experiment is needed.

In the preceding paper **CITE FIRST PAPER**, a theoretical basis by which the nonuniformities in the test gas

*DPhil Candidate, Department of Engineering Science, Oxford Thermofluids Institute, University of Oxford.
†DPhil Candidate, Department of Engineering Science, Oxford Thermofluids Institute, University of Oxford.
‡DPhil Candidate, Department of Engineering Science, Oxford Thermofluids Institute, University of Oxford.
§Research Associate, Department of Engineering Science, Oxford Thermofluids Institute, University of Oxford.
¶Associate Professor, Oxford Thermofluids Institute, Department of Engineering Science, University of Oxford.
‖Associate Professor, Oxford Thermofluids Institute, Department of Engineering Science, University of Oxford.

produced by non-ideal effects in shock tubes was detailed. The code thus developed was entitled the LAgrange Shock Tube Analysis (LASTA). The shocked test gas entropy distribution is directly related to the shock speed by which each slice is processed. The enthalpy distribution is affected by both effects caused by the growth of boundary layers and by influences arising from non-ideal driver & diaphragm rupturing. The test slug total length (distance between the shock and contact discontinuity) and the ultimate position of each gas slice is also dependent on the loss of mass to the boundary layer through the Mirels effect. LASTA simulates the shocked test gas as series of gas slices tracking along the tube in a Lagrangian frame of reference, assuming thermochemical equilibrium. It takes as input a prescribed shock history down the tube, which can be directly measured in a given experiment, as well as the initial test gas pressure, temperature and composition. The previous paper showed the accuracy of this approach with validation against Navier-Stokes simulations.

This paper applies the developed LASTA code to verify its suitability and practical application across a broad range of real experiments. These are tube diameter, non-ideal driver/diaphragm effects, thermochemistry and shock speed measurement resolution. LASTA is applied to simulate real experiments from the Oxford T6 shock tunnel operated in aluminium shock tube mode for both Air and Argon test gases at speeds where dissociation and ionization will be present. The results are compared to experimental measurements of the static pressure, Pitot pressure and stagnation point heat flux histories.

II. Shock Tube Experiments

A. T6 Stalker Tunnel

The University of Oxford T6 Stalker tunnel was recently commissioned [8] for hypervelocity and high temperature experiments, and experimental data for this paper were obtained using this facility. T6 is a multi-mode free piston driven shock tunnel. It was operated in aluminium shock tube mode, which has an optional secondary driver and an expansion from 96.3 mm to 225 mm for the shock tube (Figure 1). The length of the aluminium shock tube is 6.1 m after the conical expansion. The test window is located at 6.5 m from the secondary diaphragm and the test section measurement rake is at 7.2 m from the secondary diaphragm. All shock speed measurements used in the calculations presented in this paper are taken downstream of the nozzle expansion.

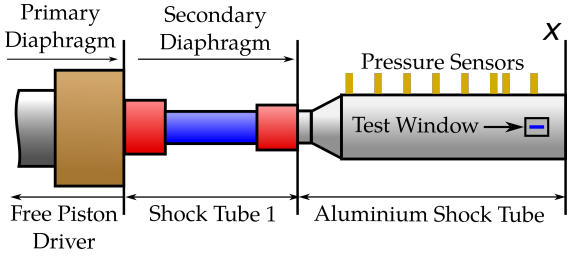

Fig. 1 Schematic of T6 with aluminium secondary tube section.

Five experiments were performed with both pure Argon and synthetic Air (21% O2, 79% N2) as test gases, at a range of fill pressures as detailed in Table 2. All data was recorded on an NI-PCIe 6368 at 2 MS/s/ch at 16 bits. Measurements of the shock time of flight are taken using wall mounted PCB113B27/28, where the arrival is assumed to be the rising edge as detected using a canny edge filter [9]. The locations of these are detailed in Table 1, as referenced from the first sensor after the expansion, STS-5, which is located at 1.46 m from the secondary diaphragm. The local shock speed is calculated as the distance between sensor locations and the time of flight between measurement locations. Shock speed calculations were performed only after STS-5. The position of the shock speed is assumed to be halfway between the sensor locations. As there is a variable sensor response and shock speed between the locations, as well as motion between the final static sensor and the Pitot sensor due to tunnel recoil, the overall uncertainty in shock speed is approximated to be 1.7% with individual uncertainties detailed in each figure. All pressure measurements have an uncertainty of ±7%, as per Hayne *et al* [10].

Table 1 Pressure transducer locations in T6.

Measurement Type	Distance from STS-5 (m)
Static Pressure	0.000
Static Pressure	1.000
Static Pressure	2.000
Static Pressure	2.970
Static Pressure	4.070
Static Pressure	4.620
Static Pressure	5.070
Static Pressure	5.270
Pitot Pressure	5.700
Stagnation Heat Flux	5.700

Measurements of the Pitot pressure and heat flux were made in the core flow at the test section rake location. Pitot pressure was measured with PCB113B24 mounted in swirl caps for protection [11]. These have a variable response due to filling time of the volume of the cavity. Stagnation point heat flux measurements were made using a novel diamond calorimeter heat transfer gauge (DHTG) developed by Penty Geraets *et al.* (2020) [12], flush-mounted in cylindrical bodies of diameter 10.50 mm and corner radius 0.13 mm. This has an effective spherical radius of 15.21 mm. In-house signal conditioning units, L1TA3, which have a bandwidth of 400 Hz were used. The measured temperature is processed into heat flux using the Sequential Function Specification Method [12]. The overall uncertainty in the heat flux is 10%.

The temperature of the tube was 20° C ±0.5 C throughout the experiment as recorded via a thermocouple on the facility. The primary and secondary driver conditions were altered to achieve the resultant shock speed profiles. Table 2 summarizes these conditions, and shows also the maximum and final shock Mach numbers to highlight the variation of

shock speed associated with each.

B. LASTA Setup

LASTA was used to simulate the T6 shots by using the experimentally recorded shock trajectories as inputs. Experimental shock speed measurements were obtained along the full length of the facility, but only the shock timing stations downstream of the nozzle were used to construct the trajectories. No information regarding the driver gas or shock behaviour upstream of the nozzle exit was required. Each simulation used 1800 time steps on the order of $5e^{-7}$ s for the Air shots, and $1e^{-6}$ s for the Argon shots. Slices were distributed every 0.25 m along a tube of radius 112.5 mm for a total length of 5.7 m. Stagnation conditions were output at 5.7 m. Static pressure traces were output at $SI5.07m$ for s215 and s218 to match the experimental wall pressure transducer there, as the transducer at 5.27 m experienced an error during those tests. Test s204 output at 5.27 m. Fill temperature and pressure were input to match the experimental conditions. All simulations assumed a laminar boundary layer. The Argon shots used a three-species Ar, Ar^+, e^- equilibrium thermochemical model, whilst the Air tests used a 9-species equilibrium Air species set consisting of N_2, O_2, N, O, NO, NO^+, N^+, O^+ and e^-. Equilibrium compositions were computed using a Gibbs free energy minimization technique following the developments of Zeleznik [13] and Huff and Morrell [14]. The equilibrium code is being locally developed as an open source resource, but has yet to be published [15]. Equilibrium wall conditions were assumed in calculation of the boundary layer properties. Heat transfer was computed using the method of Sutton and Graves [16], where the heat transfer $\dot{q}$ is found from:

$$K(H_s - h_w)\sqrt{\frac{p_s}{R}} = \dot{q} \tag{1}$$

Here, $K = 0.1113\,\mathrm{kg/s\text{-}m^{1.5}\text{-}atm^{0.5}}$ for Air and $K = 0.1495\,\mathrm{kg/s\text{-}m^{1.5}\text{-}atm^{0.5}}$ for Argon. R is the effective spherical radius, p_s is the stagnation pressure, H_s is the stagnation enthalpy, and h_w is the flow enthalpy at the cold wall.

The three-species Argon simulations consumed 6 seconds of wall clock time on a single core, whereas the 9-species Air simulations took 700 seconds on a single core. This growth in time is partly due to the use of smaller time steps with the higher speed Air tests, in addition to the many more species. It may be noted that this methodology is highly parallizable and so simulation time may be substantially reduced.

C. Argon Tests

The shock speed trajectories of each Argon test are shown in Figure 2a, with the final experimental shock speed taken at 5.5 m. Velocities shown beyond this location are the extrapolated conditions. Tests s214 and s212 contain 7% and 25% decelerations in shock speed, respectively. Figure 2b also shows the static and Pitot pressure traces from LASTA and the experiments. The LASTA simulation of the strong deceleration s212 is seen to match highly with experimental data, while a small error in measured final shock speed is estimated to increase the Pitot pressure for

Table 2 Summary of Experimental Conditions in T6

T6 Shot Number	Test Gas	Fill (Pa)
s214	Argon	67
s212	Argon	133
s218	Air	155
s204	Air	107
s215	Air	321

shot 214 slightly above the experimental value. Although the post-shock Argon is initially only 0.1% ionized, under stagnation conditions at the probe faces, the Argon becomes 1.4% ionized for s214, influencing the Pitot and heat transfer measurements, particularly near the rear of the test slug. In s212, the ionization ranges to as high as 1.6% near the rear of the test slug, a variation seen in Figure 3. Despite these sources of error, the agreement between LASTA and experiment for the Argon cases is considered to be acceptable.

The agreement for the Argon tests is further strengthened by the matching of heat transfer through both tests, as seen in Figure 2d. LASTA is able to predict the rise in both cases, and shows the more substantial rise in heat transfer associated with the elevated temperatures caused by the stronger deceleration of s212.

D. Air Tests

A more complete investigation of thermochemical effects may be performed in the context of the Air tests. Figure 4 shows the Air tests' shock speed profiles and resulting test gas pressure measurements, normalized by the fill pressure p_1. Note that test s204 had an extra sensor installed 300 mm from STS-5, which is visible in its shock profile. THis normalization was performed in order to highlight the subtly different trends observable the Pitot traces of s218 and s204. The arrival of contaminating vortices is visible in s218 and s204 in the sudden presence of relatively large oscillations, denoting the end of the useful test time. For all three tests, LASTA is able to reproduce the test slug Pitot and static pressures to within experimental uncertainties. Additionally, heat flux measured experimentally for s215 is reproduced to within 3% as seen in Figure 4d. Static pressures are obtained 0.43 m upstream of the Pitot sensors, and the test gas added between these sensors accounts for the difference in test times observed between the two.

As temperature and pressure shift through the test slug, the equilibrium species must shift with them in order to produce an accurate density, and thereby Pitot pressure and heat transfer. As a result, the predicted chemical compositions which are ultimately of interest to shock tube experiments may be trusted also to be accurate if the Pitot pressure and heat transfer predictions agree with experimental data. Therefore, the strong agreement between LASTA and T6 data across heat transfer, Pitot and static pressures indicates successful capture of thermochemical variations through the test slug.

The significance of the slightly different Pitot trends between tests s218 and s204 is now examined in the context

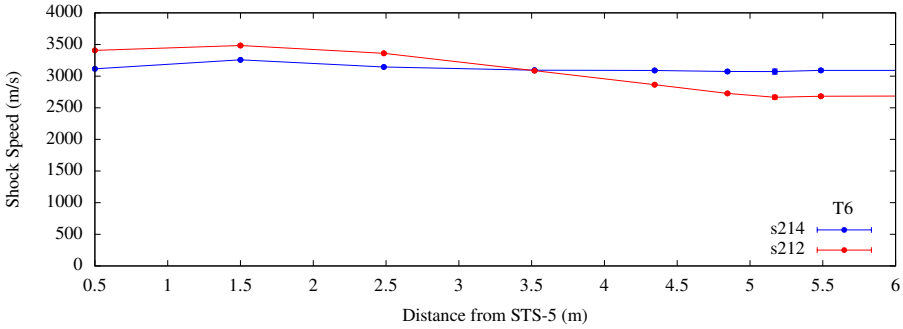

(a) Shock speed versus location for the Argon tests s214 and s212.

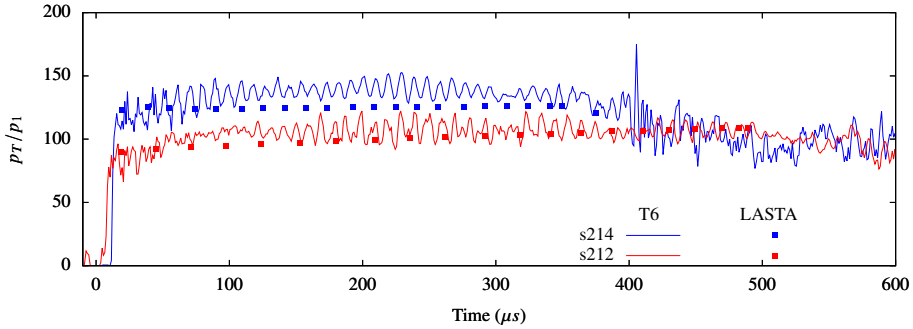

(b) Static pressure traces, normalised by fill pressure p_1 for each test at $x = 5.07$ m for s215 and s218, $x = 5.27$ m for s204.

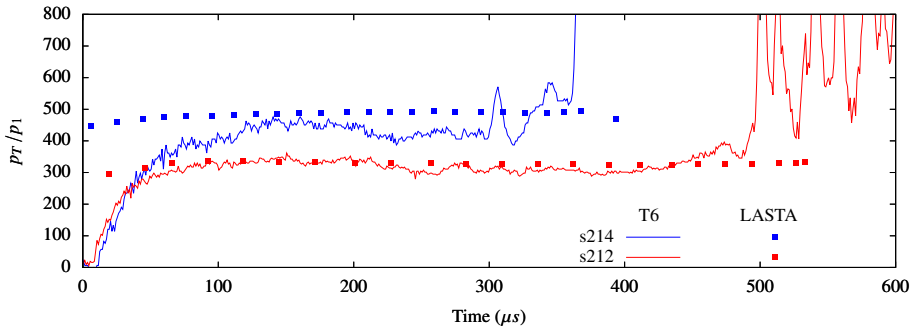

(c) Pitot pressure traces p_T, normalised by fill pressure p_1 for each test at $x = 5.70$ m.

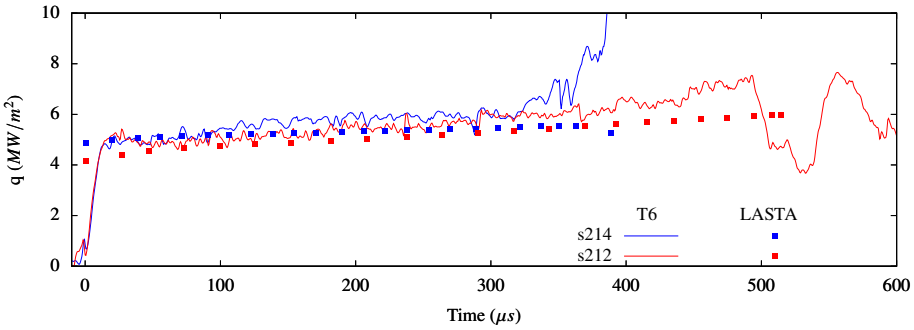

(d) Heat transfer data for each test at $x = 5.70$ m.

Fig. 2 LASTA comparison to experimental static and Pitot pressures, and heat transfer for the Argon tests.

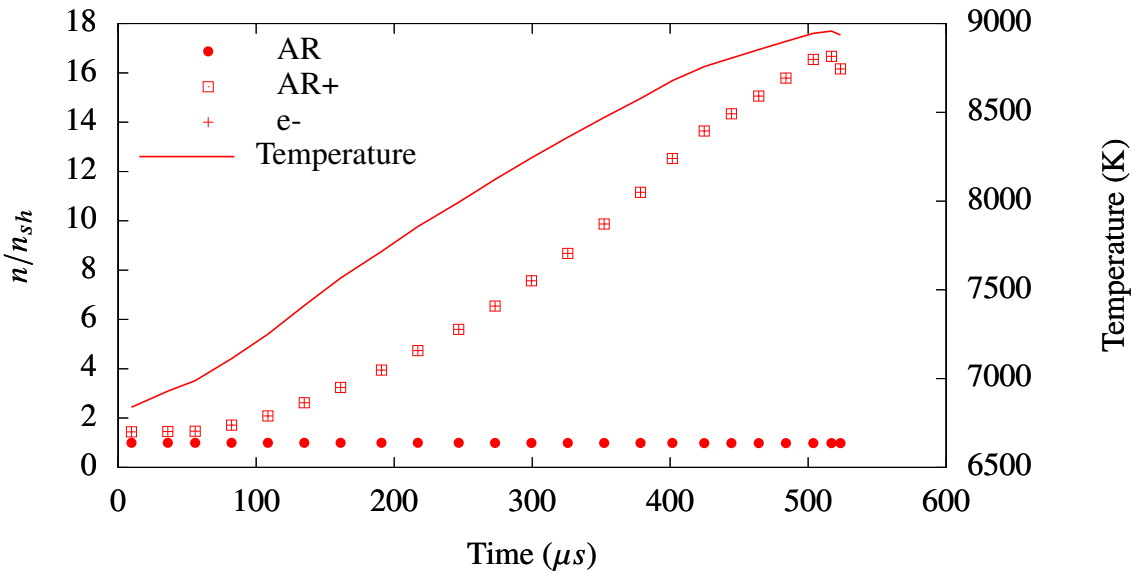

Fig. 3 Normalised variation of species' freestream moles from post-shock values in s212. Post-shock mass fraction of each species are: Ar: 9.8e-1 Ar^+: 1.5e-2 e^-: 1.5e-2 at x = 5.70 m

of thermochemistry. Figure 5 shows the variation of chemical species through the test slug both tests. A comparison between the two reveals that the extent of species variation is strongly influenced by shock speed effects. Although the two shocks arrive at the test section at a speed within 3% of one-another, the higher deceleration test s218 shows more than twice the variation in ionized species and follows an entirely different trend. The qualitative trends observed in each are also notable. It is therefore evident that the different shock trajectories produced substantially different test gas thermochemical variations.

E. Resolution of shock timing sensors

Experimental measurements of shock speed depend upon the use of fast-response sensors, typically pressure, to demark the arrival of the shock at any given distance from the diaphragm. The difference in shock arrival times at the various sensors is used to obtain shock speed measurements along the tube. The number of sensors along the tube is limited, thus a finite number of shock speed measurements are possible. As a result, the resolution of changes in shock speed may be severely limited, or missed altogether. Furthermore, a limited number of shock timing sensors can distort the computed shock trajectory in terms of the locations and magnitudes of local maxima or minima, and uncertainties exist in the shock-timing measurements themselves. Finally, each test facility has its own arrangement of shock timing sensors, and so the fundamental capacity to measure shock speed variations is different across the many laboratories. Altogether, the influence of shock speed measurement resolution must be considered.

The removal or modification of any substantial portion of the trajectory such as a local maximum which occurred

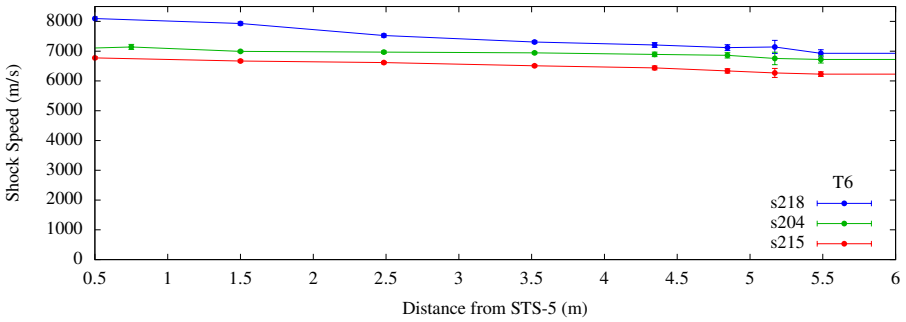

(a) Shock speed versus location for the Air tests.

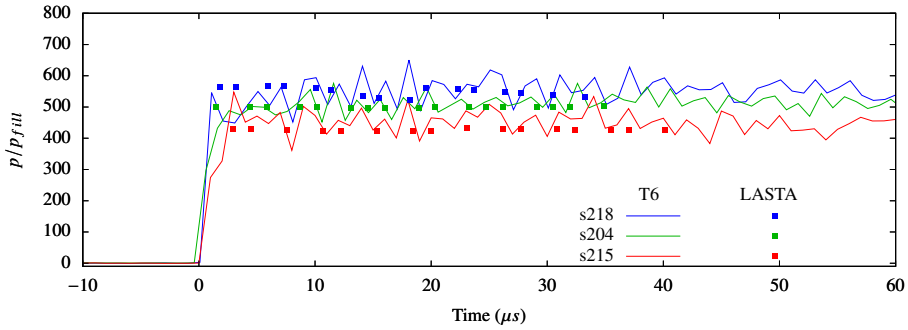

(b) Static pressure traces, normalised by fill pressure for each test at x = 5.27 m.

.75

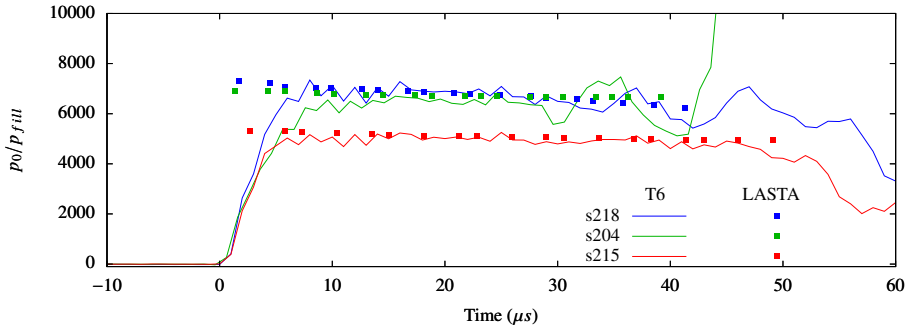

(c) Pitot pressure traces, normalised by fill pressure for each test at x = 5.70 m.

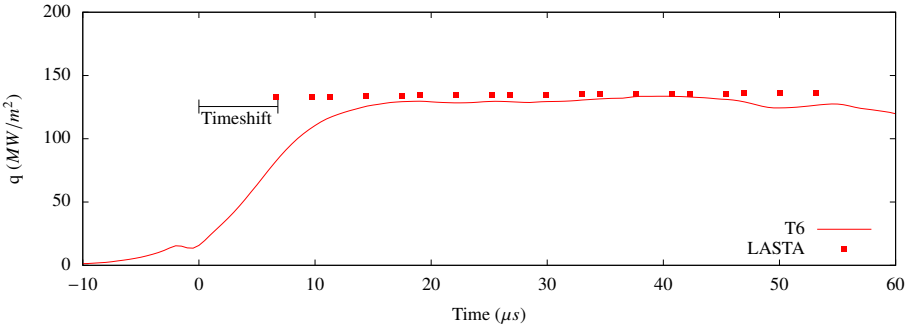

(d) Heat transfer for s215 at x = 5.70 m. LASTA results time shifted by 7 μs to account for rise time of DHTG.

Fig. 4 LASTA comparison to experimental data for the Air tests.

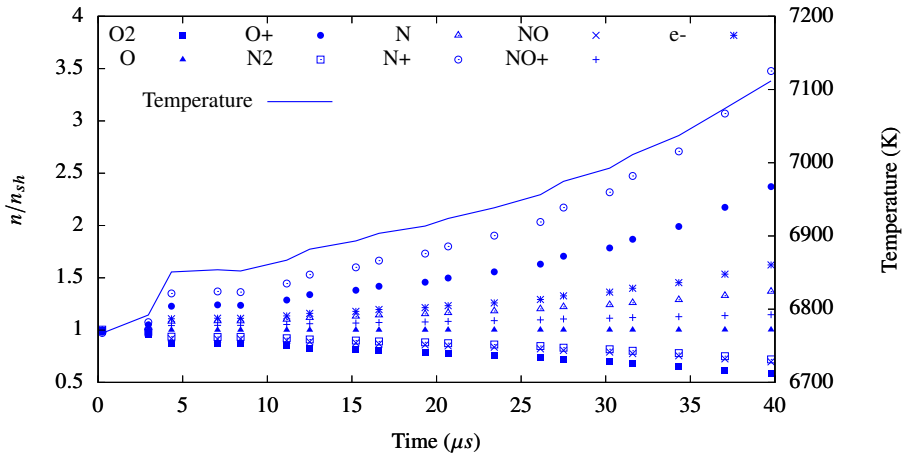

(a) Normalised variation of species' freestream number densities from post-shock values in s218. Post-shock moles of each species are: O2: 4.18e-5, O:4.2e-1, O+: 1.8e-4, N2: 3.2e-1, N: 9.3e-1, N+: 4.5e-4, NO: 3.4e-3, NO+ 7.2e-4, e-: 1.3e-3

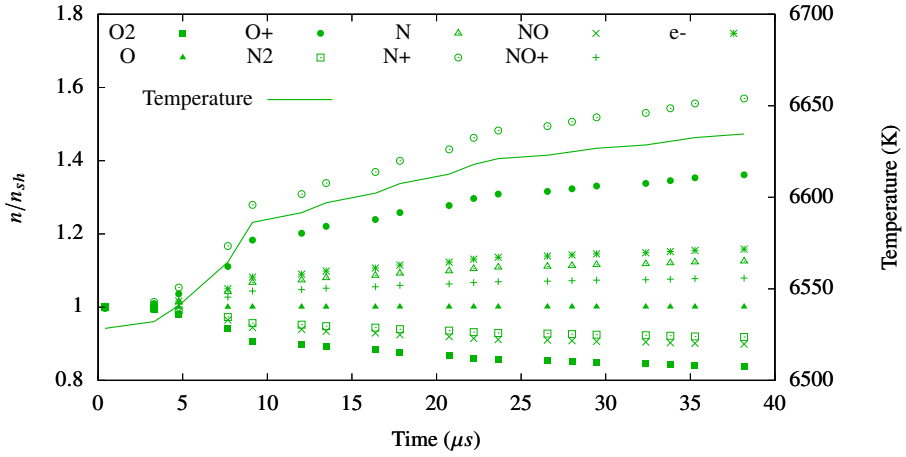

(b) Normalised variation of species' freestream number densities from post-shock values in s204. Post-shock moles of each species are: O2: 5.6e-5, O:4.2e-1, O+: 7.5e-5, N2: 4.4e-1, N: 7.0e-1, N+: 4.5e-4, NO: 4.1e-3, NO+ 5.9e-4, e-: 7.9e-4

Fig. 5 Comparison of thermochemical variations through the test slugs of tests s218 and s204.

between two sensors will result in the removal of that entropy level from the test slug. Such an absence will also introduce a degree of uncertainty in the distribution of slices due to the loss of pressure variations influencing the boundary layer thickness during the missing maximum. Since the mass balance between core flow and boundary layer is highly sensitive to pressure variations, the absence of a given portion of the trajectory may cause gas slices either to persist longer than they should, or prematurely cause the boundary layer to consume all mass from a slice, eliminating it from the test slug and thereby advancing the contact discontinuity towards the shock.

To capture this effect, a shock trajectory through Air typical of T6 experiments was selected using a relatively high resolution of sensors every 0.1 m, and LASTA was run against this trajectory as a baseline. Different trajectories were then obtained by progressively removing sensors, and so each unique trajectory was determined by integrating the time of arrival between the remaining known sensors. The sensor resolutions used were: 0.1 m, 1.0 m, 2.0 m, 5.0 m,

and also a case where only two sensors at the end of the tube were used for a final shock speed. The fill pressure for these cases was 100 Pa, and the tube diameter was 100 mm. The evident dependence of observed shock trajectory upon measurement limitations is presented in Figure 6a.

Figure 6 shows the shock trajectories, and temperature & pressure profiles through the test slug. It is evident that both the predicted test time and test gas properties are strongly influenced by the number and placement of shock timing sensors for shock speed integration. The 1 m resolution is able to largely capture the trajectory, but lacks the nuance of the full-resolution case, and so predicts slightly different trends and a peak temperature 1% lower. The difference in pressure is slightly more pronounced, showing a 2% maximum difference. The significance of these differences is seen in Figure 6d, which shows the variation of electron density through each test slug. The 1 m resolution generally obtains strong agreement, and the differences are generally qualitative in nature. However, the small differences in pressure and temperature lead to a 9% greater maximum electron density through the test slug, caused mostly by substantial variations in ionised Nitrogen and Oxygen. These variations are seen for the full resolution case in Figure 7. The other shock trajectories neither qualitatively nor quantitatively approach the variations observed in the full resolution case. It is thus clear that, in order to accurately characterise experimental test flows, the shock trajectory must be sufficiently resolved.

F. Comparison of LASTA to Alternative Methods

Using the high resolution shock trajectory from Figure 6a, the property variations through the test slug as computed using the LASTA methodology were compared against four other predictions. The first alternative prediction was to account for entropy variations as well as boundary layer effects, but not allowing for the influence of wave effects, such as was proposed by Light [3]. The second prediction was using boundary layer effects only, such as predicted by Mirels [2] and versions of which are presently common practice. This methodology is also equivalent to a stagnation-line computation without the three-dimensional effects which are often accommodated in such computations. The third alternative simply takes the post-shock properties and holds them constsant for each slice, where the locations are defined as those obtained by the Mirels computation. This concept is similar to that proposed by Brandis *et al* [17], although it may be noted that use of constant post-shock velocities results in slices actually passing the decelerating shock. The final comparison is against a uniform test slug as predicted by the final shock speed, versions of which assumption are also common in shock tube studies. Figure 8 shows the resulting variations. Figures 8a and 8b show the temperature and pressure, respectively. The resulting variation in electron number density is seen in Figure 8c. Finally, Figure 8d plots the entropy for each slice, colored by its original location in the shock tube so that it is evident from what portion of the shock trajectory each slice originated.

Removing wave effects from the LASTA methodology substantially changes both the magnitude of the nonuniformities and also the test time as the boundary layer mass balance responds to the higher pressures and temperatures. This is most apparent in the pressures, where relaxation effects produce a remarkably different pressure distribution than

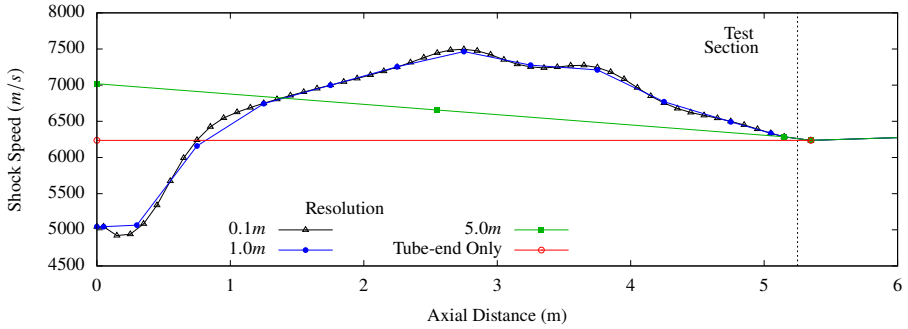

(a) Shock speed profiles derived from coarse speed measurements from the same baseline shock speed profile.

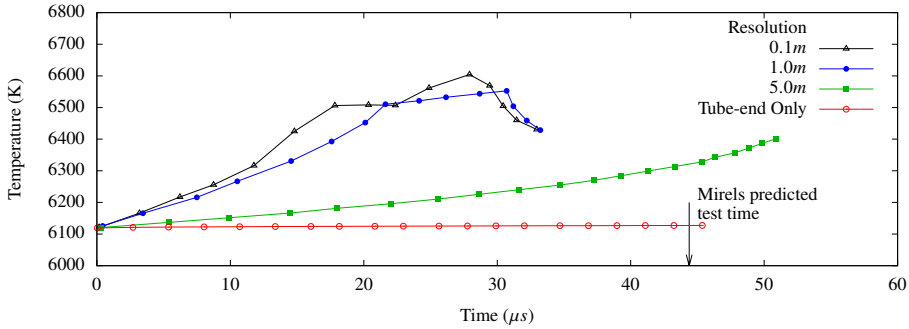

(b) Test gas temperature profiles.

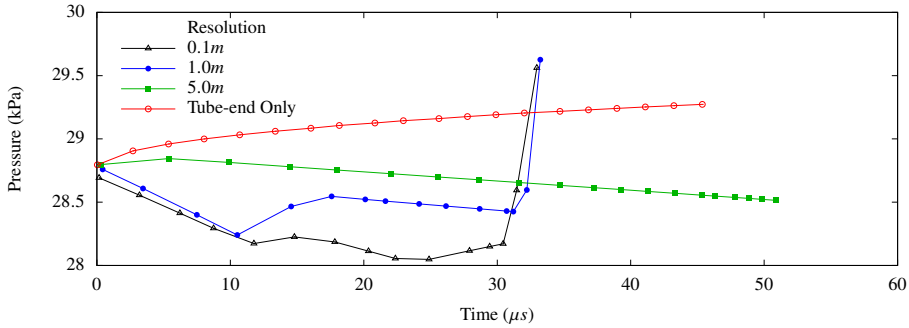

(c) Test gas pressure profiles.

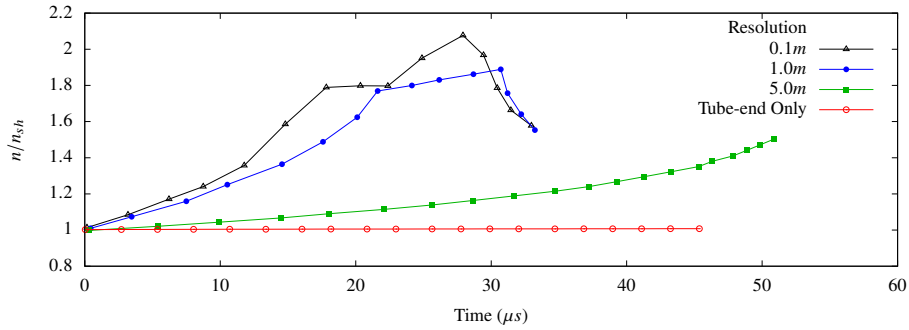

(d) Test gas ratio of slice electron number density to post-shock electron number density.

Fig. 6 The influence of limited experimental shock speed measurements. Measurement location was 5.25 m.

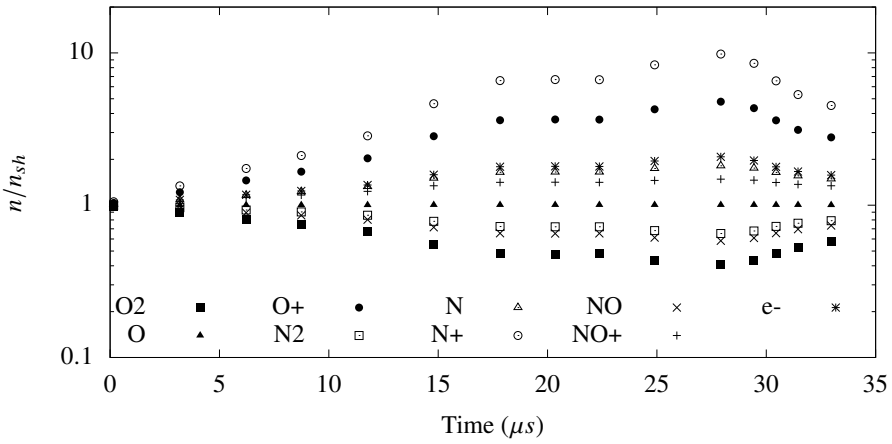

Fig. 7 Ratio of species number density to post-shock species number density for the full resolution case. Semi-log scale on y-axis. Post-shock moles of each species are: O2: 1.4e-4, O:4.1e-1, O+: 9.2e-6, N2: 6.3e-1, N: 3.1e-1, N+: 5.5e-6, NO: 6.5e-3, NO+ 3.1e-4, e-: 3.1e-4

the full LASTA prediction. Examining the entropy-only case, it is clear that by decoupling the variable post-shock properties from the boundary layer mass balance, the post-shock properties are preserved while the test time is extended considerably. This is exacerbated in part because more slices persist until the end of the tube as their mass flow is sufficient to avoid being consumed entirely by the boundary layer. This is also seen in Figure 8d by comparing the entropy levels of each slice against its originating and final locations. The most significant effect of boundary layer mass consumption is to redistribute the entropy produced by shock speed variation, and it is evident that the coupling of wave effects plays a substantial role in the boundary layer mass balance. The enthalpy recovery of the Mirels' methodology is seen to produce, for this trajectory, minimal variation away from the uniform test slug. This is due to the comparatively thin boundary layer for this case, whereas a more narrow tube or a lower fill pressure would produce more significant Mirels-type variations.

G. Tube Diameter

The influence of tube diameter upon test slug properties for a highly varying shock speed history is now examined. Four diameters were run: 25 mm, 50 mm, 100 mm, and 200 mm. Figure 9 shows that the larger diameter tubes asymptotically increase the test time, consistent with the predictions of Mirels. Test time predictions according to the methodology of Mirels [1] are shown in dotted lines. The varying shock speed shortens the test times considerably when compared to those predicted by Mirels' theory from the final shock speed. The narrowest tube is seen to most closely match Mirels' predictions, which is caused by the domination of the flow area by boundary layer effects. The same boundary layer mass flow relative to the diminished core mass flow causes the case to approach the Mirels' limit in which the entire shock-processed mass flow is consumed by the boundary layer, thereby determining the length of the test slug.

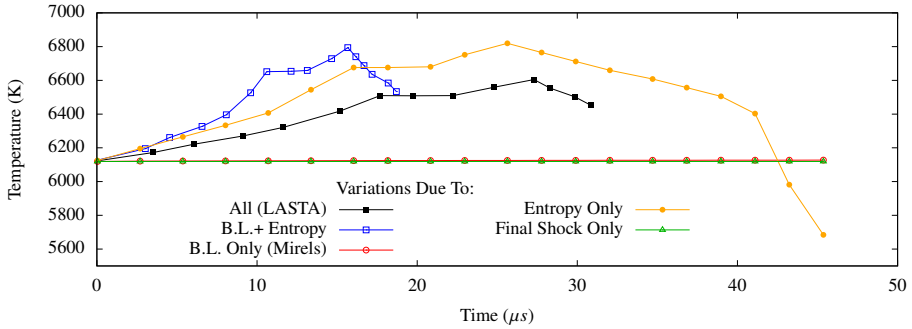

(a) Temperature profiles.

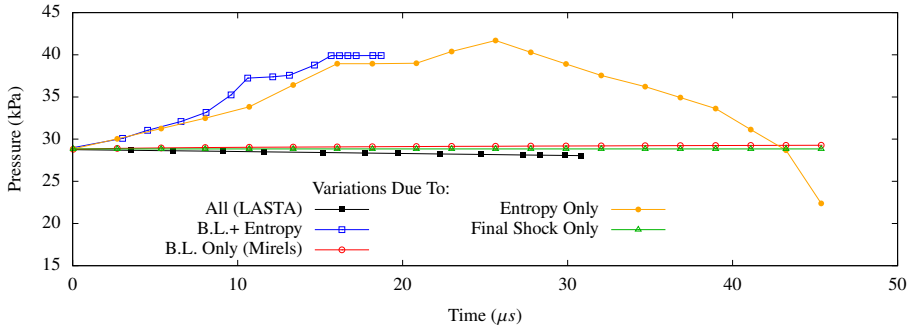

(b) Pressure profiles.

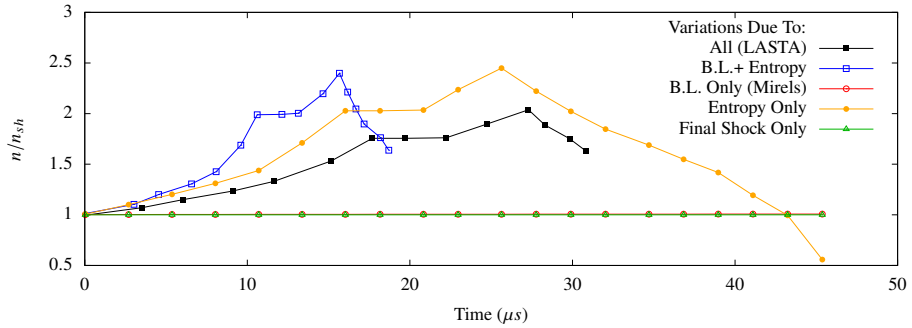

(c) Normalised electron number densities.

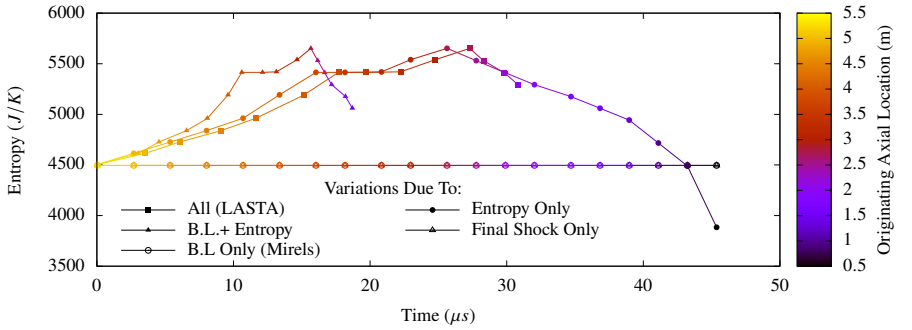

(d) Entropy profiles, colored by originating axial location.

Fig. 8 A comparison of test slug temperature nonuniformities from different analysis methodologies.

As the test time changes, the trends in temperature are largely maintained, but 'stretched' or 'compressed' according to the distribution produced by variations in speed. A small degree of variation in peak temperature is also noticeable with decreased tube diameter. This effect is due to the constriction of the stream tube by the boundary layer. Although minor under the present conditions, this effect would become more significant with a turbulent boundary layer or a lower pressure fill pressure, either of which conditions result in thicker boundary layers.

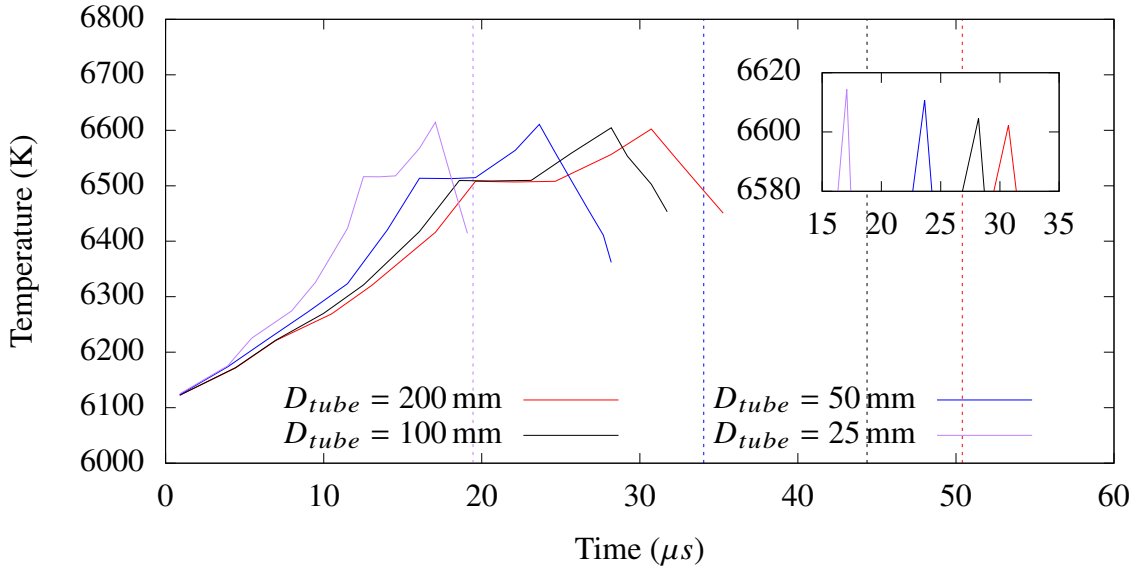

Fig. 9 Temperature profiles in the baseline shock trajectory when performed in tubes of varying diameters. Dotted lines are predictions of test time utilising Mirels' methodology [1].

III. Conclusions and Future Work

This paper applied a novel analytical methodology to characterise test gases in experimental shock tube flows where non-ideal effects were present. This work used LASTA to assess the sources of thermochemical variations through experimental test slugs, and demonstrated that shock history plays a dominant role in determining the observed thermochemical properties such that the unsteady test gas properties may be entirely derived from shock history alone. It was found that accurate measurement of the experimental shock speed profile is crucially dependent upon the experimental use of a sufficient number of shock-timing transducers along the length of the tube. Incomplete information about shock trajectory was found to influence anticipated test time and thermochemical variations through the test slug. Tube diameter was found to influence test slug nonuniformities both by changing the overall test time and also by altering the magnitude of wave and boundary layer effects associated with shock speed variation. This influence is expected to increase with a turbulent boundary layer.

A manifest extension of the work would be to apply a nonequilibrium model to the evolution of each slice in order to obtain results for higher speed shocks which produce substantial portions of nonequilibrium flow within the test slug.

Such an application would allow improved characterisation of the chemical relaxation rates which are used to inform numerical simulations of hypersonic flows and are crucial to thermal protection system design.

Appendix

Mirels [1] developed a methodology for determining the test time in a shock tube experiment based upon laminar boundary layer theory. The analysis method assumes a shock of constant speed, and determines the distance behind the shock at which the boundary layer has consumed all mass flow processed by the shock. This distance necessarily demarks the location of the contact discontinuity, and so concludes the test slug. The test time is then determined by use of the approximation that the contact discontinuity is traveling at the same speed as the shock. Thus, the test time is found as the time it takes for a particle to travel the test slug length at the speed of the shock. The maximum test slug length takes some time to develop as the shock traverses the tube, and so Mirels' analysis included a means of computing the test time at any given distance down the tube after burst. The following algorithm is based upon that provided in the UQ Gas Dynamics Toolkit [18], which is derived from Mirels [1].

The maximum test slug length l_m is given as:

$$l_m = \frac{d^2}{18\beta^2}\left(\frac{\rho_{e,0}}{\rho_{w,e0}}\right)^2 \frac{u_{e,0}}{u_w - u_{e,0}} \frac{u_{e,0}}{\nu_{w,0}} \tag{A1}$$

Here, subscript $_{e,0}$ denotes core flow properties behind the shock, u_w is the shock speed in the laboratory frame of reference, and $u_{e,0}$ is the post-shock flow speed in the shock frame of reference. Subscript $_w$ denotes wall properties, which assume a cold wall. β is found from the relation:

$$\beta = 1.59C^{0.37}\left(1 + \frac{1.796 + 0.802W}{W^2 - 1}\right) \tag{A2}$$

where

$$C = \left(\frac{\rho_e \mu_e}{\rho_w \mu_w}\right)_0 \tag{A3}$$

The term W is a measure of shock strength, given as the ratio of post-shock velocity in the shock frame of reference to shock speed $w = \frac{u_{e,0}}{u_w}$.

Knowing the maximum test slug length, the slug length l_t behind the shock when it is at any particular distance from the diaphragm is found at each shock location x_s by iterative solution of the relationship:

$$-\frac{1}{2}X = ln(1 - T^{0.5}) + T^{0.5} \tag{A4}$$

where $X = \frac{x_s}{W l_m}$ and $T = \frac{l_t}{l_m}$. The test time at each shock location down the tube is then found as $t_{test} = l_t / u_w$.

IV. Acknowledgements

The authors would like to thank the US Air Force for their support of this effort.

References

[1] Mirels, H., "Test Time in Low-Pressure Shock Tubes," *Physics of Fluids*, Vol. 6, No. 9, 1963, pp. 1201–1214. https://doi.org/10.1063/1.1706887.

[2] Mirels, H., "Flow Nonuniformity in Shock Tubes Operating at Maximum Test Times," *Physics of Fluids*, Vol. 9, No. 10, 1966, p. 1907. https://doi.org/10.1063/1.1761542.

[3] Light, G. C., "Test Gas Properties Behind a Decelerating Shock Wave in a Shock Tube," *Physics of Fluids*, Vol. 16, No. 5, 1973, p. 624. https://doi.org/10.1063/1.1694397.

[4] Holbeche, T. A., and Spence, D. A., "A Theoretical and Experimental Investigation of Temperature Variation Behind Attenuating Shock Waves," *Proceedings of the Royal Society of London. Series A, Mathematical and Physical Sciences*, Vol. 279, No. 1376, 1964, pp. 111–128. URL http://www.jstor.org/stable/2414836.

[5] Petersen, E. L., and Hanson, R. K., "Nonideal Effects Behind Reflected Shock Waves in a High-Pressure Shock Tube," *Shock Waves*, Vol. 10, No. 6, 2001, pp. 405–420.

[6] Cruden, B. A., Brandis, A. M., and Prabhu, D. K., "Compositional Dependence of Radiance in CO2/N2/Ar Systems," *44th AIAA Thermophysics Conference*, American Institute of Aeronautics and Astronautics, 2013. https://doi.org/10.2514/6.2013-2502.

[7] Satchell, M., Mare, L. D., and McGilvray, M., "Flow Non-Uniformities Behind Accelerating Shockwaves in Shock Tubes," *AIAA Scitech 2021 Forum*, American Institute of Aeronautics and Astronautics, 2021. https://doi.org/10.2514/6.2021-0649, URL https://doi.org/10.2514/6.2021-0649.

[8] Collen, P. L., Doherty, L., McGilvray, M., Naved, I., Geraets, R. T. P., Hermann, T. A., Morgan, R. G., and Gildfind, D., "Computations of High Enthalpy Shock-waves in Electric Arc Shock-Tube (EAST) at NASA Ames," *57th AIAA Aerospace Sciences Meeting*, American Institute of Aeronautics and Astronautics, 2019. https://doi.org/10.2514/6.2019-1941.

[9] James, C., "Using a Simplified Canny Edge Detector to Detect Shock Arrival in Expansion Tubes and Shock Tunnels," *Proceedings of the 32nd International Symposium on Shock Waves (ISSW32 2019)*, Research Publishing Services, 2019. https://doi.org/10.3850/978-981-11-2730-4_0031-cd, URL https://doi.org/10.3850/978-981-11-2730-4_0031-cd.

[10] Hayne, M. J., Mee, D. J., Gai, S. L., Stewart, B. S., and Morgan, R. G., "Flow Establishment Over Rearward-Facing Steps in High Enthalpy Flows," *Shock Waves*, Springer Berlin Heidelberg, 2005, pp. 173–178. https://doi.org/10.1007/978-3-540-27009-6_23, URL https://doi.org/10.1007/978-3-540-27009-6_23.

[11] McGilvray, M., Austin, J. M., Sharma, M., Jacobs, P. A., and Morgan, R. G., "Diagnostic modelling of an expansion tube operating condition," *Shock Waves*, Vol. 19, No. 1, 2009, pp. 59–66. https://doi.org/10.1007/s00193-009-0187-9, URL https://doi.org/10.1007/s00193-009-0187-9.

[12] Penty Geraets, R. T., McGilvray, M., Doherty, L. J., Morgan, R. G., James, C. M., , and Buttsworth, D. R., "Development of a fast-response diamond calorimeter heat transfer gauge," *Journal of Thermophysics and Heat Transfer*, Vol. 34, 2020, pp. 193–202.

[13] Zeleznik, F. J., and Gordon, S., "Calculation of Complex Chemical Equilibria," *Industrial & Engineering Chemistry*, Vol. 60, No. 6, 1968, pp. 27–57. https://doi.org/10.1021/ie50702a006.

[14] Huff, V., and Morrell, V., "General Method for Computation of Equilibrium Composition and Temperature of Chemical Reactions," *NASA-TN-2113*, 1950.

[15] Clarke, J., Satchell, M., and di Mare, L., "Oxford Chemical and Thermodynamics Library," , 2021. Not yet submitted.

[16] Sutton, K., and Graves, R., "A General Stagnation-Point Convective-Heating Equation for Arbitrary Gas Mixtures," *NASA TR R-376*, 1971.

[17] Brandis, A., Cruden, B., Prabhu, D., Bose, D., McGilvray, M., Morgan, R., and Morgan, R., "Analysis of Air Radiation Measurements Obtained in the EAST and X2 Shocktube Facilities," *10th AIAA/ASME Joint Thermophysics and Heat Transfer Conference*, American Institute of Aeronautics and Astronautics, 2010. https://doi.org/10.2514/6.2010-4510.

[18] Jacobs, P., Gollan, R., Damm, K., Chan, W., Gibbons, N., Jahn, I., Zander, F., Veeraragavan, A., and Wheatley, V., "The Gas Dynamics Tool Kit," http://cfcfd.mechmining.uq.edu.au/docs/tools/, 2021. Accessed: 2021-05-14.